QUANTITATION OF JUNCTIONAL AND EXTRAJUNCTIONAL ACETYLCHOLINE RECEPTORS BY ELECTRON MICROSCOPE AUTORADIOGRAPHY AFTER ^{125}I-α-BUNGAROTOXIN BINDING AT MOUSE NEUROMUSCULAR JUNCTIONS

HELEN C. FERTUCK and MIRIAM MARK SALPETER

From the School of Applied and Engineering Physics, and Section of Neurobiology and Behavior, Cornell University, Ithaca, New York 14853. Dr. Fertuck's present address is the Department of Zoology, University of Toronto, Toronto, Ontario, Canada.

ABSTRACT

The distribution and quantitation of ^{125}I-α-bungarotoxin (α-BTX) binding sites and thus acetylcholine receptor (AChR) were determined in mouse sternomastoid muscle by electron microscope autoradiography. We found that a valid criterion for receptor saturation at the neuromuscular junction was the complete elimination of neurally evoked tetanic muscle contractions, since, when such a criterion was used for the endpoint of toxin incubation, α-BTX was bound to ~90% of total available endplate sites. When, without implying localization, the presynaptic axonal membrane was used as a convenient reference structure, the concentration of α-BTX relative to this membrane was determined to be 46,000 ± 27% sites/μm^2.

By testing various hypothetical models the distribution of developed grains was found to be consistent with the hypothesis that the main acetylcholine-receptive surface coincides with the electron-dense, thickened portion of the junctional fold membrane situated at the juxtaneuronal region of the folds and dipping ~2,200 Å down the folds. The concentration of α-BTX binding sites was then calculated to be ~30,500 ± 27% sites/μm^2 of this postsynaptic dense membrane.

There was a sharp gradient in α-BTX binding extrajunctionally, with the concentration decreasing to ~4% of the subsynaptic value within 1 μm from the edge of an axonal terminal (bouton) to <1% within 3 μm and to <0.2% beyond 7 μm from that terminal. Below 4,000 Å (i.e. half-way from the top of the junctional folds) the concentration of α-BTX was also about 3% of the peak subsynaptic value. The binding density at the bottom of the junctional folds is thus comparable to extrajunctional sarcolemma at equal distance from a nerve terminal. The molecular organization at the neuromuscular junction relative to its function is discussed.

In neuromuscular junctions of vertebrate twitch muscle, the motor axon bifurcates terminally and ends in numerous elongated boutons within gutters formed by the invaginations of the muscle surface. Characteristic of the subneural muscle membrane are deep infoldings (junctional folds) which extend into the muscle for about 0.5-1.0 μm. Junctional folds are absent in the interneuronal regions of the

endplate. Histochemical and electron microscope (EM) autoradiographic studies have indicated that acetylcholinesterase (AChE) is present over the entire depth of the folds (12, 15, 38, 45, 46, 47). It was generally assumed that the acetylcholine receptor (AChR) was similarly distributed. However, until the discovery by Chang and Lee (10) that α-bungarotoxin (α-BTX) from the snake *Bungarus multicinctus* binds specifically and essentially irreversibly to the acetylcholine receptor, no direct method existed for localizing and quantifying the receptor on a fine-structural level.

The first subcellular study of receptor localization at the vertebrate neuromuscular junction was reported by Barnard and his colleagues (30, 31) who used [³H]α-BTX and electron microscope autoradiography on mouse diaphragm and reported that the receptor was distributed uniformly from the tips to the depths of the postjunctional folds. Subsequently, Fertuck and Salpeter (21) and Albuquerque et al. (2) found that the α-BTX binding sites are not uniformly distributed throughout the folds but are concentrated in the juxtaneuronal region of the folds. Additional evidence in support of the nonuniform nature of the junctional fold membranes comes from freeze-fracture studies of Rash and Ellisman (33), Heuser et al. (24), and Peper et al. (27), and the fine-structural studies of Rosenbluth (36).

Both Fertuck and Salpeter (21) and Porter and Barnard (29) have suggested that a zone of electron-dense, thickened membrane at the juxtaneuronal region of the subneural junctional folds may represent the acetylcholine-receptive surface. Although plausible, this hypothesis remained to be verified. In the present study we first used theoretical grain distributions expected from ¹²⁵I sources to test and confirm this hypothesis. We then determined the number of α-BTX binding sites per square micrometer of the subneural electron-dense membrane as well as per square micrometer of extrajunctional membrane.

MATERIALS AND METHODS

α-Bungarotoxin

Crude venom was obtained from the Miami Serpentarium and α-BTX was purified by the method of Eldefrawi and Fertuck (19) and iodinated with iodine-125 by the lactoperoxidase method of David (17). Three different batches of α-BTX were used in these studies. The specific activities obtained ranged from 38 to 135 Ci/mM. The potency and specific activity of the ¹²⁵I-α-BTX were determined by competition for acetylcholine

binding to isolated electroplax membranes from *Torpedo marmorata*.[1]

Preparation of Tissue

Five mice were used in this study. In two mice the sternomastoid muscle of the anesthetized animals was exposed by an incision in the neck, and ¹²⁵I-α-BTX $(0.8-1.6 \times 10^{-8}$ M) was applied topically until a complete block of neurally evoked tetanic muscle contraction was obtained (see reference 23). To determine when this physiological endpoint was reached, the uncut nerve was intermittently stimulated once every 15 min via a suction electrode. Stimulating frequencies of 80-100 Hz (i.e. well above the tetanic fusion frequency of $\sim$70 Hz) were used. The voltage was adjusted for each animal to produce maximum amplitude of the tetanic contraction. Muscle contraction was monitored by deflection of a needle inserted into the muscle and attached to an isotonic transducer which in turn was connected to a pen recorder. For each animal we used a different batch of α-BTX. Inactivation of tetanic responses usually took approximately 2 h (about 1.5 times longer than to inactivate single twitch responses).

A third animal was treated as described above but it died after only 90% elimination of tetanic contraction was achieved. (Such treatment need not be lethal, however, since after full inactivation of tetanic response animals can survive and eventually (by $\sim$4-8 days) recover full physiological response [23].)

Two other animals were used to determine the extent of saturation with α-BTX achieved by the physiological criterion, i.e. after the elimination of neurally evoked tetanus. In these animals the tetanic response was first eliminated as described above but with nonradioactive α-BTX. Subsequently, the muscles were bathed for an additional 2 h in ¹²⁵I-α-BTX either at the same concentration (animal 1) or at 20 times higher concentration (animal 2).

In all five animals the muscles were rinsed in Kreb's Ringer's and fixed with 1.5% glutaraldehyde in phosphate buffer by intravascular perfusion. The muscle band, expected to be rich in endplates, was dissected out and cut into small blocks. The tissue blocks were postfixed in 1% OsO₄, block stained in 1% uranyl acetate, and embedded in Epon 812. For each animal two different tissue blocks were chosen randomly from the muscle mass, and sections from three different regions of each block were prepared for electron microscope autoradiography. Our sample of endplates was thus chosen randomly from different depths in the muscle and did not allow us to distinguish between endplates at the surface and those in the interior portions of the muscle.

Electron Microscope Autoradiography

The "flat substrate" procedure of Salpeter and Bachmann (39, 40) was used, with special precautions required

---

[1] We thank Peter Ravdin for preparing the α-BTX, and Dr. M. E. Eldefrawi for the electroplax membranes.

for quantitative analysis: pale gold sections were collected onto collodion-coated slides. The thickness of about 20% of the sections was then measured with an incident light interferometer (Nomarski attachment to the Reichert Zetopan microscope) to insure that the sections were within 10% of 1,000 Å in thickness. The sections were then stained with 2% aqueous uranyl acetate for 3 h, coated with ~50 Å of carbon, and then coated with closely packed monolayers of either Ilford L4 (deep purple interference color) (Ilford Ltd., Essex, U. K.) or an improved Kodak NTE-type emulsion[2] (pale gold interference color) (Eastman Kodak Co., Rochester, N. Y.). (Emulsion interference colors were first judged on test slides taken into white light, see reference 40.)

After exposure periods ranging from 3 days to 6 wk, the Ilford L4 autoradiograms were developed in a gold latensification Elon ascorbic acid developer (GEAS) at 20°C (40), and the Kodak NTE-type autoradiograms were developed for 2 min at 24°C with Dektol (diluted 1:2 in water). The specimens were then fixed in nonhardening fixer, washed and stripped onto a water surface, picked up on electron microscope grids, and examined in a Philips 201 electron microscope.

The percent efficiency of this procedure with iodine-125 has been obtained and found to be about a factor of two to three better than for tritium, i.e. 60% for Ilford L4 (22) and 25% for the improved NTE-type emulsion (Salpeter and Szabo, manuscript in preparation). The resolution of these specimens was determined by using a modification of the radioactive line source previously employed for tritium (41). The HD value (i.e. distance from the line source containing 50% of the grains due to the source) was found to be ~800 Å for the Ilford L4 and ~500 Å for the improved NTE-type-coated specimen used in this study, and thus about two to three times better than that attainable for practical use with tritium using current techniques (Salpeter et al, manuscript in preparation).

Analysis of Autoradiograms

To localize the radioactive source, electron microscope autoradiograms were analyzed by either the density distribution or the probability circle method (see reference 43) as given in Results. Autoradiograms coated with Kodak NTE-type emulsion for optimum resolution were used for the localization. At least one grid, randomly chosen from each of the different levels sectioned, was fully scanned and all endplate profiles were photographed and enlarged photographically to 41,500 X. Only those endplate profiles in which the plane of section

---

was perpendicular to the presynaptic axonal membrane were used for these analyses. Additional grids from each block were then scanned until over 700 grains were accumulated.

For absolute quantitation of α-BTX sites per square micrometer of membrane, we used both Ilford L4 and Kodak NTE-type coated autoradiograms sampled as described above. All endplate profiles were photographed and enlarged to a final magnification of 20,000. Grain density (i.e. grains per square micrometer of membrane) was first obtained by counting developed grains within the autoradiogram and then dividing these by the surface area of the particular membrane. Measurements of membrane length were made by counting the number of times the lines from a two-dimensional grid placed over the autoradiograms intersected the membrane, and then using the equation

$$L = d \times a/2 \times \pi/2, \qquad (1)$$

where L = length of membrane, d = spacing of the grid (in micrometers at the magnification of the autoradiograms), and a = the number of intersections. (We have found that the value obtained for the length of the axonal or junctional fold membrane by this formula is within 10% of that obtained when using a map measurer or a computer.) The surface area of a membrane can then be calculated by multiplying this length by the measured thickness of the section. (This assumes that the membrane was sectioned at right angles. Therefore, for maximum validity one must include in the grain density tabulation only those autoradiograms which are judged to be so oriented by the crispness of the membrane image and, in the case of the endplate, by the thickness and crispness of the primary cleft.)

The concentration of α-BTX binding sites was then calculated from the tabulated grain density by the following equation (modified from reference 22):

$$\text{sites}/\mu m^2 = \frac{G \times d}{124,800(1 - e^{-0.01155t})} \times \frac{A}{S_oC}, \qquad (2)$$

where G = grain density (e.g., grains per square micrometer of membrane surface area), d = decays needed for one developed grain (calculated from percent efficiency values), t = exposure time in days, S_o = specific activity of the ^{125}I-α-BTX at the beginning of the exposure period (Curies per millimole), C = disintegrations per minute or 2.22×10^{12}, A = Avogadro's number in same units as used for S_o (e.g., 6.023×10^{20} molecules per millimole).

RESULTS

Localization of Junctional αBTX Binding Sites

Fig. 1 is an electron micrograph of a nerve terminal (bouton) region of a neuromuscular junction. It illustrates a characteristic feature of the

subneural muscle membrane, i.e. a differential staining of the junctional folds whereby the membrane at the top and part way down the folds appears thicker and more electron dense after lead (or other heavy metal) staining than it does in the depths of the folds. Radiating fibrils are also visible on the cytoplasmic side of these dense membranes. This increased density and thickening is especially prominent in the constricted regions or necks of the secondary clefts. For the sternomastoid muscles we determined that, on the average, the electron-dense membrane dips down the folds for about 2,200 Å (the depth of the folds in this muscle is, on the average, about 8,000 Å) and that this thickened membrane comprises about 25–30% of the total junctional fold membrane. There are also occasionally unconnected patches of densely staining membrane at various distances down the folds. Such staining properties of the junctional fold membrane have already been described by Birks et al. (5) in the frog, and these authors suggested that increased membrane thickness may represent special protein-rich regions.

EM autoradiograms of maximum resolution such as illustrated in Fig. 2 were used to determine the distribution of radioactivity within the junctional folds. The first analytic method used was the "grain density distribution method" of Salpeter et al. (41) (see also reference 43). A line parallel to the axonal membrane was drawn tangential to the tops (crests) of the junctional folds, and an experimental grain density histogram was constructed by plotting grains per unit area with distance on either side of that line.[3] The resultant

---

[3] All grains within 0.5 μm (21 mm) on the axonal side and 1 μm (42 mm) on the muscle side of the line were included in the tabulation. The perpendicular distance from every developed grain center (i.e. center of smallest circle which could circumscribe the grain) to the line was first measured (at 0.1-mm intervals) and a grain distribution histogram (total grains per unit distance from the membrane) plotted for distances on both the axonal and muscle side of the line.

In order to express the data as grain density (grains per unit area), a correction for area was determined as follows. A square grid on a plastic sheet was placed over the print being analyzed. A pin was used to punch through the plastic sheet to transfer the grid intersections to the print. The resulting lattice of points was then tabulated in the same manner and within the same distance from the line as were the grains. A point distribution histogram (total points per unit distance from the membrane) was plotted for distances on both the axonal and muscle sides of the line. A least squares fit

experimental histogram is presented in Fig. 3. This histogram confirms our previous qualitative observations (21) that the developed grains distribute themselves asymmetrically around the top of the junctional folds with most of the grains in a narrow band on the muscle (junctional fold) side of the zero line. The grain density falls off quickly on the axonal side of the line as well as towards the bottom of the junctional fold.

However, because of the spread of radiation around radioactive sources, grain density reflects, but is not identical with concentration of radioactivity. The exact distribution of the α-BTX sites must be determined by a comparison between the observed experimental grain distributions and those that are expected from hypothetical distributions of radioactivity.

One hypothesis that we tested was that the grain distribution is a result of radioactivity (i.e. α-BTX binding) uniformly distributed along the thickened, densely staining membrane of the junctional folds. (The "dense membrane" extends, on the average, ~2,200 Å down the folds.) This "dense membrane" region of the folds can be considered as a composite radioactive source consisting of a line source at the top of the junctional folds (i.e. that part of the junctional fold which is parallel to the axonal membrane) plus a band source, ~2,000 Å or 4 HD wide, extending from this line down into the folds. If the radioactivity is coincident with, and uniformly distributed along all the junctional fold membrane within this 2,000 Å depth, then the relative amount of radioactivity contributed by the line and band sources would be proportional to the relative lengths of the junctional fold membrane in these two components. Because of the scalloped nature of the postsynaptic membrane, it was difficult to define precisely where the

---

through this histogram gave a better estimate of the area of any given distance than the measured grid points which were subject to sampling errors. (The least squares fit could be used since the boundaries within which grid points were measured were perpendicular to the line at the top of the folds, and the enclosed area was thus a rough approximation of a sector of a circular area. Therefore, the area represented by histogram columns of equal width are expected to increase linearly with distance from the line at the top of the folds.) Using this smoothed distribution of grid points, we divided the number of grains in each histogram column by the number of points in the same histogram column. Thus, a grain density distribution was obtained. The histogram column widths were plotted in units of HD (500 Å for this specimen).
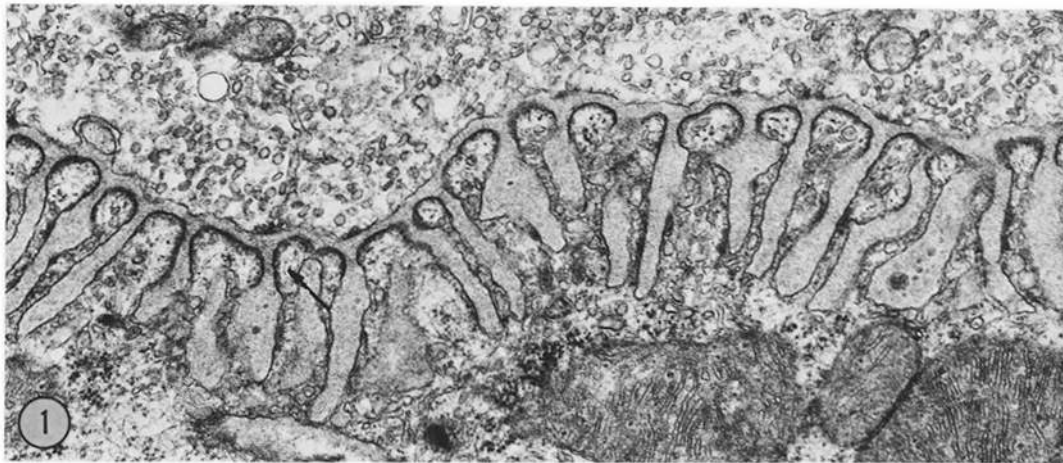
FIGURE 1   Section of neuromuscular junction of mouse sternomastoid muscle after lead citrate staining, showing a nerve terminal and subneural apparatus. Note increased membrane density and thickening at top of junctional folds and dipping partly down the folds (arrow). Note also fibrous network radiating into cytoplasm from these densities. *JF*, junctional folds; *A*, axon terminal. × 25,500.

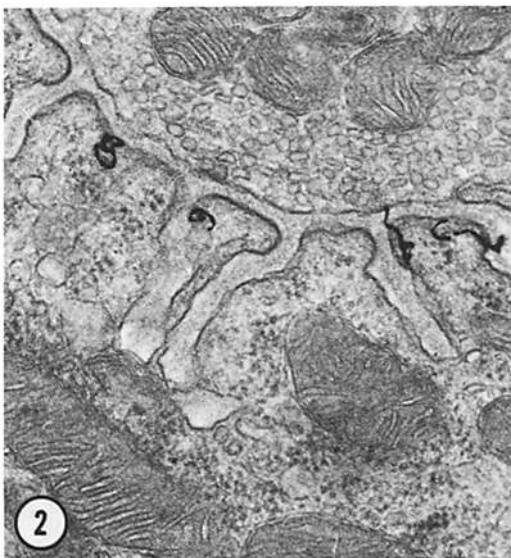FIGURE 2   High-resolution EM autoradiogram of neuromuscular junction labeled with ^{125}I-α-BTX, such as was used to construct histogram in Fig. 3, showing concentration of grains at the top of the junctional folds. 1,000-Å section and improved Kodak NTE-type emulsion. × 37,500.

demarcation is between that portion of the junctional fold membrane which is along the top of the folds (line source) and that which is dipping down the folds (band source). To construct our model source we used the average ratio of membrane lengths in the line and band of 1:1.5. We thus had a

hypothetical composite radioactive source in which 60% of the radioactivity was distributed within a 4HD band (from the top of the folds down) and 40% was in a line along the top edge parallel to the axonal membrane.

A formula and a set of curves are given by Salpeter et al. (reference 41, Fig. 17 and pp. 12–19) for generating expected grain distributions for composite sources consisting, for instance, of bands with an additional label along their edges. Using a modification of this formula[4] in conjunction with recently obtained universal curves for iodine-125-labeled sources (Fig. 4) (Salpeter et al., manuscript in preparation), we constructed the theorectical smooth curve given in Fig. 3. The expected distribution fits the histogram on the axonal side and the top 2,000 Å (4 HD) zone of the junctional folds, but falls slightly below the experimental histograms beyond that distance, espe-

---

[4] The equation, modified from Salpeter et al. (41), for a band with only one edge additionally labeled is:

$$r = q/DR(1\text{-}q), \qquad (3)$$

where 2r is the ratio of total radioactivity contributed by the band to that contributed by one edge only (in our case when the ratio of band to line of 1.5:1; $r = 0.75$); DR is a density ratio, obtained from Fig. 17 of Salpeter et al. (41) which depends on the size of source (in our case with the band of 2 HD half-width, the DR = 0.65); and q is the fraction of the normalized universal density curve for the solid band which is to be added to the fraction (1-q) of the normalized density curve of the line source.
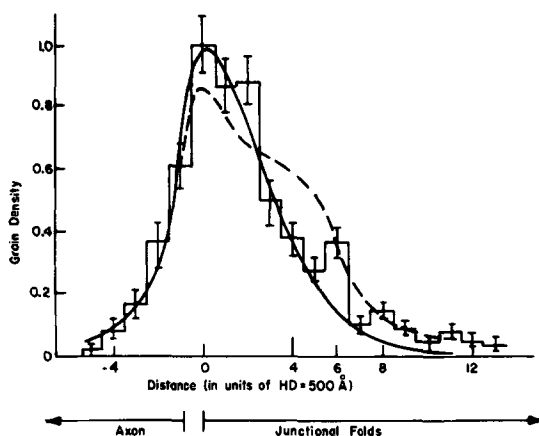
FIGURE 3 Histogram based on 747 grains, plotting grain density (grains/unit area) with distance from a line (o) drawn along the top of the junctional folds.[3] The error bars represent the sampling error. The histogram is normalized to unit density at the origin (muscle background, which is 0.017 on this scale, was not subtracted). The smooth curve superimposed on the histogram represents the expected grain distribution if only the top 2,000 Å (4 HD) of the junctional fold membrane constitutes the receptive surface. (For a description of the model source, see text and footnote 4.) The expected distribution is normalized for equal area as the experimental histogram under the 4 HD band. The dashed curve represents expected grain distribution if radioactivity extended to 3,000 Å (6 HD) down the folds (curve normalized to have equal area as experimental histogram under 6 HD band). Both hypothetical distributions peak at the origin since they represent radioactive sources with two components. A band of radioactivity dipping down the folds to 2,000 Å (4 HD) or 3,000 Å (6 HD), respectively, and an additional linear component along the crests of the folds (0 HD).

cially between 2,000 Å and 4,000 Å. (This suggests that the bulk of the radioactivity is distributed within the top 2,000 Å of the folds, but that some real radioactivity also exists below the top 2,000 Å.)

To explore the extent of the excess radioactivity beyond 2,000 Å, we constructed a second theoretical curve (dashed curve, Fig. 3) to test the assumption that the radioactivity extended uniformly for an additional 1,000 Å (i.e. was uniformly distributed along the top of the junctional folds and down the folds for 3,000 Å). The expected ratio of radioactivity on the top line source (crests of folds) and throughout the band source was again determined by the relative length of the junctional fold membrane in these two
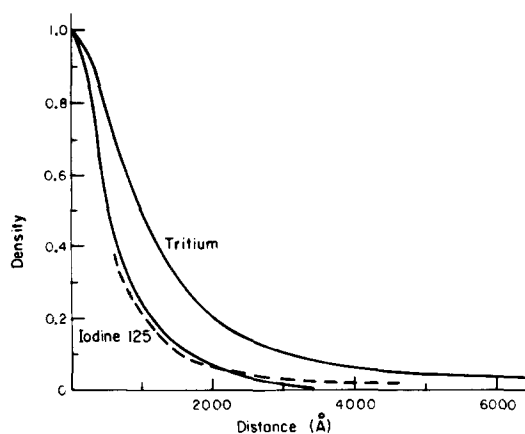
FIGURE 4 Comparative resolution and grain distribution for tritium and iodine-125 line sources (from Salpeter et al., manuscript in preparation). Both specimens are 1,000-Å sections and Kodak NTE-type emulsion. For these conditions, the HD of iodine-125 is 500 Å and of tritium is 1,000 Å. Dashed curve represents a curve with the general shape as seen for tritium but with the HD of iodine-125, illustrating the somewhat longer tail on the tritium curve.

components (and was 1:2.25). It can be seen from Fig. 3 that this second expected distribution (dashed curve) gives a considerably poorer fit to the experimental histogram (the bimodal nature of this curve is due to the relatively greater contribution of the band component). Comparing our two hypothetical distributions with our experimental histogram, we conclude that, if the receptor is distributed with a uniform concentration, then this uniformly labeled source must end somewhere between 2,000 Å and 3,000 Å down the folds. Any real label beyond the 2,000-3,000-Å depth must be at a considerably lower concentration.

Alternate Analysis and Label at Bottom of Junctional Folds

The second analysis of the experimental grain distribution used the "probability circle method" (43). This allows a comparison between grains per unit length of membrane at different distances from the top of the folds and, in particular, is an accurate quantitative assessment of the relative label at the bottom of the junctional fold membrane where the folds become sparse. Such an analysis is presented in Table I. Data for Table I were obtained as follows. Using the same autoradiograms that were used to obtain the experimental histogram in Fig. 3, we first made circles of 1

TABLE I

Grain Density Due to ^{125}I-α-BTX Binding in the Subneural Apparatus

	Density* (circled grains/circled points)			Relative area "on" vs. "off" junctional fold membranes§
Zones	Expected from 2,000-Å model source‡	"On" junctional fold membrane	"Off" junctional fold membrane	
1 Top of folds ±500 Å	3.14	3.14 ± 0.32	—	
2 500–2,000 Å	2.27	2.34 ± 0.34	3.24 ± 0.5	1.6
3 2,000–4,000 Å	0.44	0.68 ± 0.14	0.68 ± 0.18	1.8
4 4,000 Å to bottom of folds	0.07	0.16 ± 0.04	0.09 ± 0.03	1.2

* "On" junctional fold membrane means within a 1-HD (500 A) zone either side of a junctional fold membrane profile. "Off" junctional fold membrane means beyond 1 HD from a junctional fold membrane profile. Muscle background density of 0.06 was subtracted from these values.

‡ Based on hypothesis that radioactivity is distributed uniformly on dense junctional fold membrane and ends abruptly at 2,000 Å from top (zone 3). Values are comparable to those in smooth curve (Fig. 3) but normalized to units comparable to those in this Table.

§ Relative area was obtained from the relative number of circled points "on" and "off" junctional fold membrane. These values show that the junctional fold membranes, especially in the top 4,000 Å of the folds, are too closely stacked to be resolved autoradiographically, thus explaining the nonsignificant difference in grain density "on" and "off" junctional fold membrane.

‖ Since circles around grain centers and grid points were of 500-Å radius, there could, by definition, be no circled grains or points "off" junctional fold in zone 1.

HD (500 Å) radius around the center of every developed grain (circled grains); then similar-size circles were drawn around every intersection point (circled points) in a square grid. The region of the junctional folds was then divided into four zones from zone 1 which was ±500 Å either side of the zero line (i.e., line drawn along crests of junctional folds) to zone 4 which was between 4,000 Å from the top of the folds and a line drawn along the bottom of the folds. Both the grains and the points were tabulated as to whether their surrounding circle overlapped a junctional fold membrane ("on" membrane) or not ("off" fold membrane. This method of tabulation in essence separated the number of developed grains found within a 1-HD rim of a junctional fold membrane (and thus per unit length of membrane) from those found beyond that rim. The relative grain density at different distances down the folds was obtained from the ratio of circled grains to circled points "on" junctional fold membrane (column 2, Table I).

The data in Table I confirm and expand the conclusions drawn from Fig. 3. The grain density "on" junctional fold membrane (i.e. per unit length of junctional fold membrane) stays relatively constant in zones 1 and 2 (down to 2,000 Å) which are coincident with the region of dense junctional fold membranes, and then drops rapidly, remaining, however, somewhat higher than

expected if the source ended abruptly at 2,000 Å (see column 1). If one subtracts the expected grain density due to radiation spread from our 2,000-Å band model source, the residual grain density in zone 3 (2,000–4,000 Å down the folds) is ~9% and in zone 4 (below 4,000 Å down the folds) is ~3% of the value at the top of the folds (zone 1).

Presynaptic Label

The possibility of some presynaptic α-BTX labeling has been raised in immunohistochemical studies (16). The EM autoradiographic procedure is limited by its resolution, which, even for iodine-125 and the NTE emulsion used here, is ~500 Å, thus just marginal for resolving presynaptic axonal from postsynaptic membrane, since the primary cleft is also about 500 Å. Composite curves based on the hypothesis that a certain fraction of the radioactivity is located on the axonal membrane suggest that the axonal label, if any, does not exceed 10–20% of the total. However, even 10% of total radioactivity could still represent a sizable site density (i.e., it would be at a concentration as high as 25% of that on the postsynaptic membrane). Although, on the basis of denervation studies, Porter and Barnard (28) reported an exclusively postsynaptic localization of label the EM autoradiographic method as used in that study is not sensitive enough to detect even

a 20% decrease in total radioactivity. Similarly, the resolution in the study by Bourgeois et al. (6) is insufficient to establish an exclusively postsynaptic localization. Thus, the question of whether presynaptic sites exist or not, and at what site density, must await further investigation.

Absolute Quantitation of Junctional Receptors

We approached the problem of determining the concentration of α-BTX binding sites in the neuromuscular junction by a two-stage process. First, we correlated the number of α-BTX sites with the size of the presynaptic axonal membrane. (Presynaptic axonal membrane is here defined as that region of the axonal membrane adjacent to the postsynaptic junctional fold; see Fig. 5.) The relation, sites per square micrometer of presynaptic membrane, was not intended to imply localization, which would be incompatible with the results reported above. We chose presynaptic membrane area since it is easily defined and measured, is stable, and provides a convenient subcellular normalizing unit from

which other molecular relationships can be calculated, and which allows easy comparisons between animals under various experimental conditions. Once the number of sites per square micrometer of presynaptic membrane was established, we obtained the ratio of presynaptic to postsynaptic dense membrane and then calculated the sites per square micrometer of the latter membrane.

These tabulations were performed as follows: short-exposure autoradiograms were sampled and photographed as described in Materials and Methods. Grains within the distance from the primary cleft included in the histogram illustrated in Fig. 3, i.e. 0.5 μm on the axonal side and 1 μm on the muscle side of the primary cleft, were counted for this tabulation. Muscle background was subtracted. The surface area of the presynaptic axonal membrane was then obtained as described in Eq. (1) and text in Materials and Methods, and the number of grains was divided by this area to get grains per square micrometer of membrane surface area. From this grain density, we calculated the concentration of α-BTX binding sites per
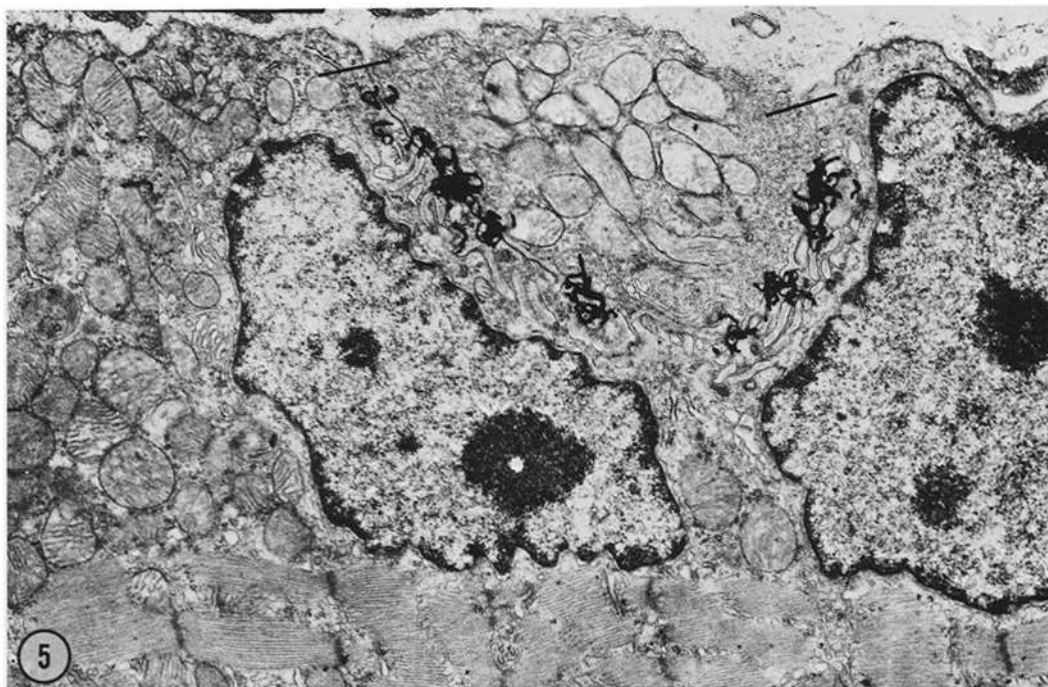

FIGURE 5   Overexposed EM autoradiogram (Ilford L4 emulsion) of neuromuscular junction, showing sharp localization of label at subneural region. Both the extrajunctional sarcolemma and the bottom of junctional folds have an equally low density of label. The presynaptic axonal membrane is defined in this study as that region of the axonal membrane adjacent to the postsynaptic junctional folds (bounded by lines). Extrajunctional sarcolemma begins just beyond the axonal membrane. × 11,800.

TABLE II

| Method of labeling | No. animals | No. grains | Sites/μm^2 $\times$ 10^{-3} | |
			of presynaptic membrane	of postsynaptic* dense membrane
100% inactivation of tetanus by ^{125}I-α-BTX	2	1,575	44.0 $\pm$ 27%	25–31
90% inactivation of tetanus by ^{125}I-α-BTX	1	510	39	22–28
Residual sites:				
100% inactivation with nonradioactive α-BTX → ^{125}I-α-BTX for 2 h	2	502	2.5 $\pm$ 50%	1.5–1.8
Total sites:				
(100% inactivation + residual sites)			46.5 $\pm$ 27%	26–33 $\pm$ 27%

* Obtained by dividing sites/square micrometer of presynaptic membrane by 1.5–1.8 which is the factor by which the area of the postsynaptic electron-dense membrane exceeds that of the presynaptic membrane.

square micrometer of presynaptic axonal membrane using Eq. (2), also given in Materials and Methods.

The quantitative data are summarized in Table II. We found that:

(a) in the two animals that were fixed after complete elimination of neurally evoked tetanic contraction, the average concentration of α-BTX per square micrometer of presynaptic membrane was 44,000 $\pm$ 10,000.

(b) in the animal that died after only 90% elimination of tetanic contraction, the α-BTX concentration per square micrometer of presynaptic axonal membrane was 38,000, thus within the animal to animal variation range seen after 100% elimination of response;

(c) the ratio of presynaptic axonal to postsynaptic electron-dense membrane was roughly between 1:1.4 and 1:1.8. Thus, at 100% inactivation of tetanus, the average concentration of α-BTX sites per square micrometer of postsynaptic electron-dense membrane is calculated to be ~28,000 $\pm$ 27%;

(d) in the two animals labeled with ^{125}I-α-BTX after 100% elimination of neurally evoked tetanus with nonradioactive α-BTX, we obtained, on the average, ~2,500 sites per square micrometer of presynaptic axonal membrane (to be called "postcriterion" label). A large animal to animal variation in this "postcriterion" label (4,300 and 610 sites per square micrometer) suggests that the physiological endpoint is not very strictly defined. However, since in neither animal was the "post-

criterion" label greater than 10% of total sites which could be labeled when ^{125}I-α-BTX was used to complete elimination of tetanus, we can conclude that this physiological criterion represents a reasonable measure of receptor saturation (at least 90%);[5]

(e) although no grain density histograms were constructed to localize the postcriterion sites precisely, qualitatively the developed grains were again seen to cluster at the top of the folds similarly to the clustering seen after 100% elimination of tetanus with radioactive toxin. We can thus conclude that the same juxtaneuronal localization pertains for all the sites which can be labeled with α-BTX under our experimental conditions, even when labeling is continued for twice the time needed to achieve inactivation of tetanic response. We believe that the relative absence of label at the bottom of the folds is not due to diffusion barriers, since no diffusion barriers prevent even larger molecules such as horseradish peroxidase (8), thorium dioxide (4), or dextran (9) from reaching the bottom of the junctional folds;

(f) when the average postcriterion site density is

---

[5] One should, however, be aware that since it takes some time to wash out the ^{125}I-α-BTX, substantial labeling can occur after contraction is fully blocked. One cannot therefore equate the number of sites seen to be labeled at criterion with the minimum that is needed to block contraction, but rather with an upper limit in that category. Similarly, one cannot consider the postcriterion label as "spare receptor," in which category it can only represent a lower limit.

added to the average sites per square micrometer labeled at criterion of 100% elimination of tetanus, one obtains a total of 46,500 ± 27% α-BTX sites/μm^2 of presynaptic membrane and 30,500 ± 27% α-BTX sites/μm^2 of postsynaptic dense membrane.

It should be remembered that the above-mentioned values are based on an assumption of uniform distribution of label and thus represent average site densities.

Extrajunctional α-BTX Binding

An overexposed EM autoradiogram of an axon terminal after α-BTX binding (Fig. 5) illustrates the fact that heavy labeling is restricted to the subneural regions of the endplate with essentially no obvious label on extrajunctional membrane. One could therefore not determine qualitatively whether there was any extrajunctional α-BTX binding above muscle background. (Interaxonal regions of the endplate were included in our definition of extrajunctional membrane). The following quantitative procedure was therefore adopted. Only Ilford L4 autoradiograms were used (to provide maximum sensitivity and thus grain yield). The extrajunctional membrane was divided into "distance bits" from an axonal terminal as seen in Fig. 6. The first was a 0.5-μm "bit" 0.5–1 μm from a terminal, then there were three consecutive 2-μm "bits" to 7 μm from a terminal, and
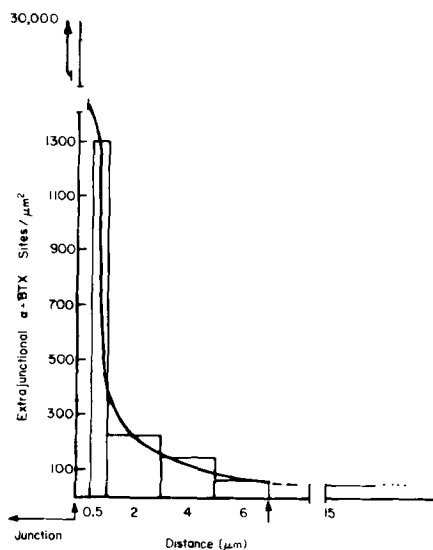

FIGURE 6   α-BTX binding density per square micrometer of extrajunctional membrane with distance from a nerve terminal.

finally membrane > 15 μm from a nerve terminal. The first 0.5 μm was not included because of difficulty in correcting for radiation spread from the highly labeled subneural membrane. For all except the 0.5- to 1.0-μm bit, we used EM autoradiograms in which the junctional subneural membrane was highly overexposed, in order to get a high enough extrajunctional grain yield for a meaningful assessment.

Grains (i.e. grain centers) were counted to 1 HD (800 Å for Ilford L4 emulsion and iodine-125) on either side of the muscle membrane, so that, per micrometer length of extrajunctional muscle membrane, grains were counted over a 0.16-μm^2 area. The value for random tissue background grains per square micrometer of tissue was determined and subtracted from this initial grain count. The grains were then related to surface area of muscle membrane (i.e. length of membrane times thickness of section) and converted to α-BTX binding sites by Eq. (2) as was previously done for the subneural sites. The final value was then multiplied by two, since grains were collected only to 1 HD from the muscle membrane and, by definition of HD, this collects exactly 50% of the grains due to such a line source (41). Only those muscle fibers were included which were separated by several HD from an adjacent fiber so as to insure that radiation spread between fibers did not have a major effect on the results.

We found a steep gradient of α-BTX binding sites with distance from a nerve terminal (see Fig. 6). The subneural site density of ~30,000/μm^2 falls to about 4% (i.e. ~1,300 sites/μm^2 in the 0.5–1.0-μm bit from the axon terminal, then to < 1% (i.e. ~224 sites/μm^2) within a 1–3-μm rim from the nerve terminal and to about 0.2% (i.e. 64 sites/μm^2) by 7 μm. This value is only slightly lower (44 sites/μm^2) beyond 15 μm from the nerve terminal. For comparison, muscle background (which was subtracted) when converted to surface area of membrane as described above is equivalent to ~32 sites/μm^2.

DISCUSSION

Localization and Quantitation of Junctional AChR

Recent studies using EM autoradiography have agreed that the α-BTX binding at the subneural apparatus is asymmetrical, being primarily concentrated at the top (juxtaneural region) of the

junctional folds. Since the EM autoradiographic label seemed to coincide with the region of the postjunctional membrane which is morphologically distinct by being thicker, more densely staining, and characterized by filaments radiating into the cytoplasm, the assumption was made in two studies (21, 29) that these densely staining membranes represent the α-BTX receptive surface. In both of these studies, average values obtained for α-BTX binding sites per square micrometer of total junctional fold membrane were then extrapolated to obtains sites per square micrometer of the specialized membrane.

In the present study the basic assumption underlying the above calculations was first tested by comparing an experimental grain distribution with that expected from a hypothetical source of radioactivity uniformly distributed and coincident with the location of the specialized dense membrane. Our results are consistent with the hypothesis that the bulk of the radioactivity is coincident with the electron-dense membranes of the junctional folds which in the sternomastoid extend, on the average, about 2,200 Å down the folds with some discontinuous bits seen as far down as 4,000–5,000 Å. (Since our autoradiographic analysis averaged the grain density over all the folds at a given distance from the top, it tends to obscure the fact that one frequently sees several developed grains linearly arranged down an individual junctional fold, whereas adjacent folds are unlabeled. Such "hot spots" need yet to be assessed statistically.)

It is important to remember that site density or label is *not* identical with grain density. A casual observer glancing over many autoradiograms of α-BTX-labeled endplates would be struck by numerous developed grains lying over axoplasm or over the bottom of the junctional folds. This point is emphasized by the number of developed grains expected at the bottom of the folds from a theoretical source at the top 2,000 Å or 3,000 Å of these folds given in Fig. 3. We must further bear in mind that Fig. 3 is based on autoradiograms with the highest resolution currently available, i.e. iodine-125 and an NTE-type emulsion (HD = 500 Å). If these data were obtained with Ilford L4 emulsion (HD $\simeq$ 800 Å), the same number of grains would be spread more than one and a half times as far from the source, and if tritium had been the source, the grains would be spread three times as far. Thus, the same fraction of total grains found within a 2,000 Å zone below the source in

our histograms in Fig. 3 would distribute over a 6000-Å zone if tritium-labeled α-BTX and Ilford L4 emulsion were used. Therefore, before one can assess the actual site density from the distribution of developed grains, careful consideration must be given to the resolution of the technique used, and the model source from which the radiation spread is being corrected.

This discussion is relevant to considering the discrepancies between our conclusions and those drawn by Porter and Barnard (29) who report that between 4 and 6 HD (i.e. 6,400–9,600 Å) down the folds in the bat diaphragm and thus below the average depth given by Porter and Barnard for these folds, the site density per square micrometer of membrane is about 16% of that found in the 0–3 HD region (0–4,800 Å). Even higher values are claimed for the mouse diaphragm (Fig. 5 of reference 29). These authors' site density at the bottom of the folds relative to the top is thus considerably higher than ours. We are not sure of the nature of this discrepancy but it may be due in part to the fact that they appear to correct for radiation spread from a source model which is a line at the top of the fold (in fact, on the axonal membrane; Fig. 3 of reference 29). Furthermore, the choice of diaphragm muscle, in which the junctional folds are shorter than they are in the sternomastoid, and the use of an autoradiographic procedure which has a threefold poorer resolution than the procedure used by us, also made it harder for them to resolve the bottom from the top of the junctional folds. A real difference between diaphragm and sternomastoid muscles must also remain a possibility.

Once the hypothesis was confirmed that the major radioactive source due to [125]-α-BTX binding is coincident with the location of the electron-dense membrane, the average local site density was determined. We first determined the site density per unit area of presynaptic axonal membrane (46,000 ± 27% site per square micrometer), using this membrane as a useful normalizing compartment. (Because this membrane is easy to identify and measure, we feel that the site density relative to it is more accurate than any subsequent extrapolation.) the concentration of α-BTX sites was then extended to the specialized dense membranes and found to be, on the average, $\sim$26,000–33,000 ± 27% sites/μ^2. This value is comparable to the 33,000 or 31,000 ± 27% sites/μ^2 given by Bourgeois et al. (6, 7) for the eel electroplax. Similar values can be extrapolated from several

studies on mouse and rat whole endplates (26, 3, 20), when the calculations of Salpeter and Eldefrawi (42) are corrected to account for our more recent understanding regarding the α-BTX localization.

Porter and Barnard (29) calculate $\sim$20,000–25,000 α-BTX sites per electron-dense membrane in a bat and mouse endplate and argue that their values may represent a fundamental difference between these mammalian and the eel synapses. This conclusion may be premature, given the uncertainties in the extent of site saturation and in the measured lengths of dense membranes, and knowing the limit of quantitative accuracy in EM autoradiography. We thus feel that 30,000 $\pm$ 8,000 α-BTX binding sites/μ^2 of postsynaptic receptive membrane remains a reasonable assessment within the accuracy of the present procedures employed, and includes the mammalian junctions as well as the eel electroplax. The possibility still exists that there are real regional differences in receptor concentrations at different endplates, but this remains to be determined.

Extrajunctional αBTX Binding

The α-BTX binding is highly concentrated at subneural regions of the endplate. A quantitative analysis demonstrates a very sharp gradient (Fig. 6) with binding site density falling to $<1\%$ (<300 sites/μ^2) its subneural value within 3 μm from a nerve bouton and to $<0.2\%$ ($\sim$60 sites/μm^2) the subneural value by 7 μm. Due to radiation spread from the junctional folds, it is more difficult to get an accurate value for the first micrometer beyond a nerve terminal. Our best value for this "rim" region (0.5–1.0 μm from the edge) is about 4% ($\sim$1,300 sites/μ^2). Interestingly, this density is about the same as the density at the junctional fold membrane below 4,000 Å from the top. The junctional fold membranes beyond the thickened specializations can thus be considered comparable to extrajunctional membrane at similar distance from the receptive surface.

A sharp localization has also been established at amphibian and reptile junctions by iontophoresis of ACh and the measured ACh sensitivity by membrane depolarization (25). Basically, the two results are very similar. Kuffler and Yoshikami (25) find that the peak subneural ACh sensitivity of 5,000 mV/nCi drops to 1–2% that value within 2–4 μm from the nerve. However, whereas in their study the extrajunctional sensitivity remains at about this value, we found an additional fivefold

drop in α-BTX by 7 μm. The difference in these two results may reflect a species difference between the amphibian endplate of the Kuffler and Yoshikami study and the mammalian enplate studied by us. However, other reasons relating to the different techniques used cannot at present be eliminated.

Molecular Organization of Neuromuscular Junction and Role of Junctional Folds in Neuromuscular Transmission

From the time these junctional folds were first described (34, 35), it was generally assumed that they functioned to increase the receptive surface area of the postsynaptic membrane. This point of view was strengthened by the mosaic model of AChE and AChR distribution proposed by Barnard et al. (3), as well as by EM autoradiographic studies claiming to demonstrate a uniform distribution of AChR over the full depth of the folds (30). Subsequently, several laboratories almost simultaneously presented data to suggest a membrane specialization at the juxtaneuronal region of the junctional folds by morphological studies (33, 36, 27) as well as evidence for a concentration of receptor in that region by EM autoradiography (21, 2). It is therefore now generally accepted that the junctional folds do not serve to increase the postsynaptic receptive surface (at least not in its full depth), and the mosaic model is now untenable.

The relationship of the junctional fold membrane to AChE is also as yet not completely clear. Previous EM autoradiographic studies on esterases at the mouse sternomastoid muscle (37, 38) have established that the distribution of the esterases covers a much broader region of the junctional folds than we now know to be the case for the α-BTX labeling. A quantitative assessment of the site density at these endplates gives values of $\sim$2,500 acetylcholinesterase sites/μ^2 of postjunctional folds (45). However, the size of the junctional folds is not tightly coupled with AChE function, since it was recently shown in studies on the extraocular muscle that junctional fold surface area is not necessarily exactly correlated with the amount of AChE sites at the endplate and thus is not involved in any simple manner in providing surface area for increased esterase need (46).

The morphology of the junctional fold membrane resembles that of other postsynaptic surfaces (nerve/nerve as well as nerve muscle) in that there

appear to be regions of dense, thickened membrane (presumably rich in AChR), as at the tops of the junctional folds, separated by membrane of normal morphology. These AChR-rich patches seem to be highly stable and there is no indication of membrane flow of receptor either in early post-denervation stages (7) or after inactivation with α-BTX (23). Since the high concentration of AChR ($\sim$30,000 sites/μ^2) present on the ACh-receptive surfaces essentially saturates the membrane surface, perhaps nearby space must be made available for other essential protein molecules such as the ATPase and other enzymes. However, this does not provide any explanation for the large variation in relative area occupied by the receptive and nonreceptive surface found in various synapses.[6]

Combining the AChE and the AChR data available for the mouse sternomastoid muscle, we see that at the ACh-receptive surface of the folds, the α-BTX site density (AChR) exceeds the AChE density by approximately, 5- to 10-fold. Although one can argue whether all the α-BTX sites represent AChR or not (11), and what fraction of sites of both molecules is present along the axonal membrane, it appears indisputable that the local concentration of AChR exceeds AChE at the top of the junctional folds and that this relationship is reversed in the depth of the folds where the AChR content drops off drastically.

It seems reasonable to suggest that the secondary clefts provide a sink for ACh diffusion where the AChE would insure destruction while leaving the choline within the subneural apparatus. This suggestion is consistent with some other morphological features of the vertebrate endplate. Presynaptically (at least in amphibians), distinct membrane specializations are believed to be associated with ACh release sites (12–14, 18). These specializations face the necks of the secondary clefts. In the mouse endplates such distinct morphological

[6] It has been suggested (29) that in the endplate the electron-dense postsynaptic membrane is a constant fraction of the total junctional fold membrane. This conclusion was, however, based on only two muscles, the diaphragm and sternomastoid, which have a relatively similar junctional fold morphology. Preliminary observations on the endplates of the mouse extraocular muscle, which has very sparse junctional fold (44, 46) and in which the dense membrane comprises somewhere between 50% and 60% of total junctional fold membrane rather than the 25–30% seen in the sternomastoid and diaphragm, lead us to dispute this generalization.

sites are not prominent. However, we occasionally see presynaptic membrane densities and they invariably face a neck of a secondary cleft as in the frog. A packet of ACh, if released towards such a postsynaptic region, would see the largest possible area of receptor surface (i.e. at both the top of the folds and that part which is dipping down the folds). Such a geometry is more interesting if one considers that for the rat, at least, where the average surface area of the presynaptic axonal membrane is 1,400 μm^2 (calculated from values in reference 42) and if the amount of ACh released per impulse is $\sim$3 $\times$ 10^6 molecules (32), or about 300 quanta of ACh, one can calculate that for a full neuromuscular response there is only one quantum (10^4 ACh molecules) released, on the average, per 5 μm^2 of presynaptic surface area. This would cause an initial nonuniform distribution of ACh in the primary cleft and produce local regions of very high ACh concentration, optimally placed to diffuse down the secondary cleft.

Due to the high concentration of AChR at the postsynaptic area, one can calculate that by the time the contents of one quantum have diffused about 2,500 Å ($\sim$0.1 ms) laterally or down a fold, it- will have seen $>$6,000 receptors and thus enough to provide the 1,000–5,000 ion channels commonly associated with a single MEPP. (It is of interest that the 2,500 Å also corresponds to the distance down the folds which contain receptor.) Our calculation is particularly appealing when we consider that within this small postsynaptic area ($\sim$0.2 μm^2) the ACh is initially present at a concentration of $>$3 $\times$ 10^{-3} M and thus will both be able to swamp the AChE and also to produce a considerable degree of AChE substrate inhibition (1). Furthermore, there is also a high probability that more than one ACh molecule can interact with one receptor (which may be necessary to open a single ion gate).

Thus, while the exact role of the secondary folds in neuromuscular transmission remains open, the accumulating data lead to an emerging picture of the molecular organization of the subneural apparatus. We essentially have a two-phase membrane consisting of AChR-rich regions or patches separated by nonreceptive membrane of unknown function and variable length. The AChR-rich patches are rigidly localized adjacent to the axonal presynaptic terminal and are sandwiched within a much wider zone of AChE of overall lower concentration. The evidence for a high concentra-

tion of AChR at the top of the junctional folds provides the basis whereby the postsynaptic response can occur over a very small area (~ 0.2 μm^2 per MEPP) after a very short diffusion time (~ 0.1 ms) and thus at a very high ACh concentration ($> 3 \times 10^{-3}$ M). This permits nonoverlapping action of ACh quanta during neuromuscular transmission and provides an explanation of how the junction can function while forcing its ACh essentially to run the gauntlet of AChE in the primary cleft before ever seeing the AChR.

REFERENCES

1. AUGUSTINSSON, K. B. 1949. Substrate concentration and specificity of choline ester-splitting enzymes. *Arch. Biochem.* **23:**111-126.
2. ALBUQUERQUE, E. X., E. A. BARNARD, C. W. PORTER, and J. E. WARNICK. 1974. The density of acetylcholine receptors and their sensitivity in the postsynaptic membrane of muscle endplates. *Proc. Natl. Acad. Sci. U.S.A.* **71:**2818-2822.
3. BARNARD, E. A., J. WIECKOWSKI, and T. H. CHIU. 1971. Cholinergic receptor molecules and cholinesterase molecules at mouse skeletal muscle junctions. *Nature (Lond.).* **234:**207-209.
4. BIRKS, R. I. 1966. The fine structure of motor nerve endings at frong myoneural junctions. *Ann. N.Y. Acad. Sci.* **135:**8-26.
5. BIRKS, R., H. E. HUXLEY, and B. KATZ. 1960. The fine structure of the neuromuscular junction of the frog. *J. Physiol.* **150:**134-144.
6. BOURGEOIS, J. P., A. RYTER, A. MENEZ, P. FROMAGEOT, P. BOQUET, and J.-P. CHANGEUX. 1972. Localization of the cholinergic receptor protein in *Electrophorus* electroplax by high resolution autoradiography. *FEBS (Fed. Eur. Biochem. Soc.). Lett.* **25:**127-133.
7. BOURGEOIS, J. P., J. L. POPOT, A. RYTER, and J.-P. CHANGEUX. 1973. Consequences of denervation on the distribution of the cholinergic (nicotinic) receptor sites from *Electeophorus electricus* revealed by high resolution autoradiography. *Brain Res.* **62:**557-563.
8. CECCARELLI, B., W. P. HURLBUT, and A. MUARO. 1972. Depletion of vesicles from frog neuromuscular junctions by prolonged tetanic stimulation. *J. Cell Biol.* **54:**30-38.
9. CECCARELLI, B. W. P. HURLBUT, and A. MAURO. 1973. Turnover of transmitter and synaptic vesicles at the frog neuromuscular junction. *J. Cell Biol.* **57:**499-524.
10. CHANG, C. C., and C. Y. LEE. 1963. Isolation of neurotoxins from the venom of *Bungarus multicinctus* and their modes of neuromuscular blocking action. *Arch. Int. Pharmacodyn. Ther.* **144:**241-257.
11. COLQUHOUN, D., and H. P. PANG. 1974. The inhibition of α-bungarotoxin binding to denervated rat mucles by tubocurarine and other drugs. *Br. J. Pharmacol.* **51:**12-13.
12. COUTEAUX, R. 1972. Structure and cytochemical characteristics of the neuromuscular junction. Int. Encyclop. of Pharmacol. and Therapeut. Section 14. Vol. I. J. Cheymol, editor. Pergamon Press, Oxford and New York. Ch. 2, 7056.
13. COUTEAUX, R., and M. PÉCOT-DECHAVASSINE. 1970. L'ouverture des vesicules synaptiques au niveau des "zones actives." Septième Congrès Internatisonale de Microscopie Electronique. Grenoble, Vol. 3. 703-710.
14. COUTEAUX, R., and M. PÉCOT-DECHAVASSINE. 1974. Les zones spécialisées des membranes presynaptiques. *C. R. Hebd. Séances Acad. Sci.* 291-293.
15. CSILLIK, B. 1965. Functional Structure of the Post-Synaptic Membrane in the Myoneural Junction. Akademiai Kiado, Budapest.
16. Daniels, M. P., and Z. Vogel. 1974. Immunoperoxidase staining of α-bungarotoxin bound to acetylcholine receptors in mouse motor end plates. *J. Cell Biol* **63** (2, Pt. 2):76 a. (Abstr.).
17. DAVID, G. S. 1972. Solid state lactoperoxidase: a highly stable enzyme for simple, gentle iodination of proteins. *Biochem. Biophys. Res. Commun.* **48:**464-471.
18. DRYER, F., K. PEPER, K. AKERT, C. SANDRI, and H. MOOR. 1973. Ultrastructure of the "active zone" in the frog neuromuscular junction. *Brain Res.* **62:** 373-380.
19. ELDEFRAWI, M. E., and H. C. FERTUCK. 1974. A rapid method for the preparation of [^{125}I]α-bungarotoxin. *Anal. Biochem.* **58:**63-70.
20. FAMBROUGH, D. M., and H. C. HARTZELL, 1972. Acetylcholine receptors: Number and distribution at neuromuscular junctions in rat diaphragm. *Science (Wash. D. C.).* **176:**189-191.
21. FERTUCK, H. C., and M. M. SALPETER. 1974. Localization of acetylcholine receptor by ^{125}I-labeled α-bungarotoxin binding at mouse motor endplates. *Proc. Natl. Acad. Sci. U.S.A.* **71:**1376-1378.
22. FERTUCK, H. C., and M. M. SALPETER. 1974. Sensitivity in EM autoradiography for ^{125}I. *J. Histochem. Cytochem.* **22:**80-87.
23. FERTUCK, H. C., W. W. WOODWARD, and M. M. SALPETER. 1975. In vivo recovery of muscle contrac-

tion after α-bungarotoxin binding. *J. Cell Biol.* **66**: 209-213.

24. HEUSER, J. E., T. S. REESE, and D. M. LANDIS. 1974. Functional changes in frog neuromuscular junction studies with freeze-fracture. *J. Neurocytol.* **3**:108-131.

25. KUFFLER, S. W., and D. YOSHIKAMI. 1975. The distribution of acetylcholine sensitivity at the post-synaptic membrane of vertebrate skeletal twitch muscles: iontophoretic mapping in the micron range. *J. Physiol.* **244**:703-730.

26. MILEDI, R., and L. T. POTTER. 1971. Acetylcholine receptors in muscle fibers. *Nature (Lond.)*. **233**:599-603.

27. PEPER, K., E. DREYER, C. SANDRI, K. AKERT, and H. MOOR. 1974. Structure and ultrastructure of the frog motor endplate. A freeze-etching study. *Cell Tissue Res.* **149**:347-455.

28. PORTER, C. W., and E. A. BARNARD. 1974. Electron microscope (EM) autoradiographic counting of acetylcholine receptor sites in mammalian motor endplates. *J. Histochem. Cytochem.* **22**:293.

29. PORTER, C. W., and E. A. BARNARD. 1975. The density of cholinergic receptors at the endplate postsynaptic membrane: ultrastructural studies in two mammalian species. *J. Membr. Biol.* **20**:31-49.

30. PORTER, C. W., E. A. BARNARD, and T. H. CHIU. 1973. The ultrastructural localization and quantitation of cholinergic receptors at the mouse motor endplate. *J. Membr. Biol.* **14**:383-401.

31. PORTER, C. W., T. H. CHIU, J. WIECKOWSKI, and E. A. BARNARD. 1973. Types and locations of cholinergic receptor-like molecules in muscle fibres. *Nat. New Biol.* **214**:3-7.

32. POTTER, L. F. 1970. Synthesis, storage and release of C^{14} acetylcholine in isolated rat diaphragm muscles. *J. Physiol.* **206**:145.

33. RASH, J. E., and M. H. ELLISMAN. 1974. Studies of excitable membranes. I. Macromolecular specializations of the neuromuscular junctional and the non-junctional sarcolemma. *J. Cell Biol.* **63**:567-586.

34. REGER, J. F. 1955. Electron microscopy of the motor endplate in rat intercostal muscle. *Anat. Rec.* **122**:1-16.

35. ROBERTSON, J. D. 1956. The ultrastructure of a reptilian myoneural junction. *J. Biophys. Biochem. Cytol.* **2**:381-394.

36. ROSENBLUTH, J. 1974. Substructure of amphibian motor endplate. Evidence for a granular component projecting from the outer surface of the receptive

membrane. *J. Cell Biol.* **62**:755-766.

37. SALPETER, M. M. 1967. Electron microscope radioautography as a quantitative tool in enzyme cytochemistry. I. The distribution of acetylcholinesterase at motor endplates of a vertebrate twitch muscle. *J. Cell Biol.* **32**:379-389.

38. SALPETER, M. M. 1969. Electron microscope radioautography as a quantitative tool in enzyme cytochemistry. II. The distribution of DFP-reactive sites at motor endplates of a vertebrate twitch muscle. *J. Cell Biol.* **42**:122-134.

39. SALPETER, M. M., and L. BACHMANN. 1964. Autoradiography with the electron microscope: A procedure for improving resolution, sensitivity and contrast. *J. Cell Biol.* **22**:469-477.

40. SALPETER, M. M., and L. BACHMANN. 1972. Electron microscope autoradiography. *In* Principles and Techniques of Electron Microscopy. Biological Applications. M. A. Hayat, editor. Van Nostrand Reinhold, New York. Vol. 2. 221-278.

41. SALPETER, M. M., L. BACHMANN, and E. E. SALPETER. 1969. Resolution in electron microscope autoradiography. *J. Cell Biol.* **41**:1-20.

42. SALPETER, M. M., and M. E. ELDEFRAWI. 1973. Sizes of endplate compartments, densities of acetylcholine receptor and other quantitative aspects of neuromuscular transmission. *J. Histochem. Cytochem.* **21**:769-778.

43. SALPETER, M. M., and F. A. McHENRY. 1973. Electron Microscope Autoradiography, Analysis of Autoradiograms. *In* Advanced Techniques of Biological Electron Microscopy. J. K. Koehler, editor. Springer-Verlag, New York. 114-151.

44. SALPETER, M. M., F. A. McHENRY, and H. FENG. 1974. Myoneural junctions in the extraocular muscles of the mouse. *Anat. Rec.* **179**:201-223.

45. SALPETER, M. M., H. PLATTNER, and A. W. ROGERS. 1972. Quantitative assay of esterases in endplates of mouse diaphragm by electron microscope autoradiography. *J. Histochem. Cytochem.* **20**: 1059-1068.

46. SALPETER, M. M., A. W. ROGERS, and F. A. McHENRY. 1976. Acetylcholinesterase in the endplate compartments of the fast extrocular muscle of the mouse. *J. Cell. Biol.* In press.

47. TERÄVÄINEN, H. 1969. Localization of acetylcholinesterase in the rat myoneural junction. *Histochemie.* **17**:162-169.

48. ZACKS, S. I. 1973. The Motor Endplate. Robert E. Krieger Publishing Co., Inc., Huntington, N.Y.